Unusually large microporous HKUST-1 via polyethylene glycol-templated synthesis: enhanced CO2 uptake with high selectivity over CH4 and N2

Fahed Aloufi, Nadhem Missaoui, Riyadh Halawani, Hamza Kahri, Bassem Jamoussi, Andrew J. Gross

Unusually large microporous HKUST-1 via polyethylene glycol-templated synthesis: Enhanced CO_2 uptake with high selectivity over CH_4 and N_2

Fahed A Aloufi[a], Nadhem Missaoui[b*], Riyadh F Halawani[a], Hamza Kahri[b], Bassem Jassoumi[c], Andrew J. Gross[d]

a Department of Environmental Sciences, Faculty of Environmental Sciences, King Abdulaziz University, Jeddah 21589, Saudi Arabia
b Laboratory of Interfaces and Advanced Materials, Faculty of Sciences, University of Monastir, Tunisia
c Department of Environment Science, Faculty of Meteorology and Arid Land Agriculture, King Abdulaziz University, Jeddah 21589, Saudi Arabia
d Department of Molecular Chemistry (DCM), Univ. Grenoble Alpes-CNRS, 38041 Grenoble, France.
*Corresponding author: missaoui.nadhem1@gmail.com

ABSTRACT

Porous solids with highly microporous structures for effective carbon dioxide uptake and separation from mixed gases are highly desirable. Here we present the use of polyethylene glycol (20,000 g/mol) as a soft template for the simple and rapid synthesis of a highly microporous Cu-BTC (denoted as HKUST-1). The polyethylene glycol-templated HKUST-1 obtained at room temperature in 10 min exhibited a very high Brunauer-Emmett-Teller (BET) surface area of 1904 m^2/g, pore volume of 0.87 cm^3/g, and average micropore size of 0.84 nm. However, conventional HKUST-1 exhibits a BET surface area of 700-1700 m^2/g. X-ray powder diffraction and electron microscopy analysis confirm the formation of highly crystalline and uniform octahedral particles with sizes ranging from 100 nm to 120 µm. Adsorption isotherms recorded at temperatures between 273 K to 353 K and pressures up to 40 bar revealed a more favorable adsorption capacity of HKUST-1 for CO_2 vs. CH_4 and N_2 (708 mg (CO_2)/g, 214 mg (CH_4)/g and 177 mg (N_2)/g at 298 K and 40 bar). The Langmuir, isotherm model and isosteric heats of adsorption were evaluated. The CO_2 interaction at PEG-templated HKUST-1 is physical, exothermic and spontaneous with $\Delta H° = -6.52$ kJ/mol, $\Delta S° = -13.72$ J/mol, $\Delta G° = -2.43$ kJ/mol at 298 K at 40 bar. The selectivities in equimolar mixtures were determined as 53 and 24, respectively, for CO_2 over N_2 and CH_4. CO_2 adsorption-desorption tests reveal high adsorbent reusability. The cost-effective and quickly prepared PEG-templated HKUST-1 demonstrates high efficacy as a gas adsorbent, particularly in selectively capturing CO_2.

Keywords: Metal organic framework; polymer templated MOF; PEG templated synthesis; carbon dioxide adsorption; methane adsorption.

1. Introduction

Global warming linked to the accumulation and generation of gases such as carbon dioxide and methane is one of the most significant problems facing the international community. The concentration of CO_2 emissions in the atmosphere has significantly increased in the past century from 280 to 400 ppm, and is expected to increase to 570 ppm by 2100. Likewise, CH_4 emissions have increased by more than double during this time [1-3]. The development of economical methods to selectively capture and adsorb CO_2 and CH_4 from the environment is necessary to alleviate the global burden. This is particularly relevant for flue gases where selective CO_2 capture and uptake is required in the presence of uncombusted N_2 [4]. The development of materials for storage/adsorption of CO_2, CH_4 and N_2, separation of CO_2/N_2 from flue gas, and separation of CO_2/CH_4 from natural gas, is essential to help combat greenhouse gas emissions [4]. Several studies on the storage and separation of CO_2, CH_4 and N_2 gases have been reported involving the use of commonly-employed porous adsorbents such as zeolites [5] and activated carbon [6]. Both zeolites and activated carbons are highly developed nanostructured porous structures that are widely used as commercial adsorbents and filters to remove contaminants including volatile organics and as well as waste gases. Microporous activated carbon, for example, has been used to effectively adsorb carbon dioxide due to its high porosity, some selectivity, and low moisture sensitivity [6, 19]. Activated carbons are also economically affordable [6, 19]. The adsorption of CO_2 was investigated to study the equilibrium and kinetic behavior utilizing activated carbons; and a maximum adsorption capacity of 10 mmol/g (440 mg(CO_2)/g) was reported for activated carbon (GCA-1240) [30].

Porous materials such as zeolites and activated carbon have a relatively high energy requirement for regeneration, and relatively limited adsorption capacities as well as selectivity for CO_2 [7, 8]. Metal organic frameworks (MOFs) are a new class of crystalline and porous materials with multi-dimensional networks formed by coordination bonds between inorganic clusters (metal ions) and diverse organic linkers (ligands) [9-11]. Their unique architectures generally offer high specific surface area and pore volume, and the possibility to tune chemical functionality and pore structure. Their attractive textural properties have resulted in them being extensively studied over the last decade for the storage and adsorption of gases such as CO_2 and CH_4, for gas separations, and for catalysis [12-15]. Amongst the MOFs, $Cu_3(BTC)_2$, (also known as MOF-199, Cu-BTC or HKUST-1) [16] is a 3-D face-centered cubic (fcc) crystal MOF formed via the association of

dimeric cupric carboxylate units with benzene-1,3,5-tricarboxylate. The cubic structure consists of octahedral cages that share paddlewheel units to define larger micropores of about 0.9 nm in diameter and smaller tetrahedral side pocket ultramicropores of about 0.5 nm in diameter. The small pores are linked to the main channels via triangular windows of about 0.35 nm diameter~~s~~ [17]. Cu-BTC (HKUST-1) MOF with its octahedral structure offers benefits for gas adsorption linked to its ~~a~~ large BET surface area, various micropore sizes, high porosity, high crystallinity, and the Lewis~~'s~~ acidity of its open metal sites [18, 19].

The HKUST-1 MOF with specific BET surface areas ranging between 692 and 1656 m^2/g can be synthesized by numerous methods; including, solvothermal [16], ultrasonic irradiation [20], microwave [21] and mechanochemical [22] methods. The high temperature syntheses and/or organic solvents used in classical solvothermal methods are commonly employed and are beneficial for high crystallinity and purity of the product. The use of high temperatures up to 523 K, the long crystallization times to achieve practical yields, typically beyond 1 day, and the presence of significant amounts of CuO and Cu_2O by-products are however undesirable [23, 24]. Nevertheless, rapid room temperature synthesis of HKUST-1 nanoparticles in 1 hour with a moderate BET surface area of 1346 $m^2.g^{-1}$ has been reported [25].

Ultrasonic irradiation and microwave techniques provide access to rapid synthesis but can be difficult to reproduce due to the use of diverse synthesis setups with variable exposure parameters [26, 27]. The facile and rapid preparation of MOFs is very attractive to facilitate fundamental studies of these materials as well as ~~towards~~ their eventual practical application in industry. Recently, we ~~have~~ started to develop room temperature synthesis methods for MOFs based on a soft polymer template approach. The use of certain polymers as templates can improve simplicity, reduce reaction times or temperatures, and improve yields, purities and reproducibility [28-30]. Numerous MOF structures have been realized by diverse methods, including polymer-templating, and assessed as potential CO_2 and CH_4 adsorbents, as summarized below in Table ~~S~~1 [28-47].

In this work, we report the synthesis of a new highly porous HKUST-1, herein referred to as PEG-templated HKUST-1, via a soft polymer template synthesis strategy, and explore its application for CO_2 and CH_4 adsorption and separation. To the best of our knowledge, this is the first time that an inexpensive polymer template such as polyethylene glycol has been used for HKUST-1 synthesis. Herein we report the optimized protocol for facile

synthesis that benefits from a short reaction time of only 10 min at room temperature and ambient pressure. Adsorption isotherms models were investigated to gain new insight into the adsorbate-adsorbent interaction. Three models were applied to understand the gas-solid adsorption mechanism. Diverse characterizations are reported to shed new light on the relationship between the pore structure and gas adsorption and separation performance. Finally, the adsorption selectivity, heat of adsorption, and regeneration performance of our adsorbent will also be presented.

2. Materials and methods

2.1 Materials

Copper nitrate ($Cu(NO_3)_2.2.5H_2O$, 99%), 1,3,5-benzenetricarboxylic acid (H_3BTC, 99%) dimethylsulfoxide (DMSO, 99%), methanol (99%), triethylamine (TEA; $(C_2H_5)_3N$; 99%) and polyethylene glycol (PEG, average molecular weight of 20,000 g/mol) were obtained from Sigma-Aldrich and used as received. The all gases used for these analyses were of high purity (99.99%) and obtained from Sigma-Aldrich.

2.2 Synthesis of PEG-templated metal organic framework adsorbent: HKUST-1

PEG-templated Cu-HKUST-1 MOF was prepared at room temperature from high-purity precursors: $Cu(NO_3)_2 \cdot 2.5H_2O$ and benzene-1,3,5-tricarboxylic acid (H_3BTC) with $PEG_{20,000}$ used as a soft template. The use of PEG was encouraged by its ability to form homogenous solutions with metallic salts via micellar and dispersion effects that in turn promote the uniform growth of MOF particles with reduced agglomeration, and have proven to provide access to higher surface area adsorbents for gas adsorption [28, 29]. The polymer is considered also to adsorb on the surface of the metal clusters and coordinated ligands, resulting in modification of crystal growth and changes in the pore structure of the resulting MOF; for example, the PEG molecules may specifically interact via hydrogen bonding with the ligand. In the first step, PEG (0.4 g) was added to DMSO (12 g) then Cu $(NO_3)_2 \cdot 2.5H_2O$ (0.177 g, 0.76 mmol) was subsequently added. The mixture was stirred for 5 min to form a well-defined suspension (solution 1). In parallel, the H_3BTC ligand (0.246 g, 1.17 mmol) was dissolved in a DMSO (12 g) solution. TEA (used as a base; 0.49 ml (3.51 mmol) was then combined with the ligand solution (solution 2). The $PEG_{20,000}$ suspension (solution 1) was then combined with ~~the~~ solution 2 and the resulting mixture stirred at room temperature for 10 min. Blue colloids formed and were subsequently collected after centrifugation (3000 rpm, 15 min), extraction, and washing five times with methanol to remove any undissolved precursors including the polymer. The blue-colored

product, HKUST-1, was finally dried in a vacuum oven at 423 K for 24 h. The resulting solid was characterized by infrared (FTIR), powder X-ray diffraction (PXRD), scanning electron microscopy (SEM), thermogravimetric analysis (TGA) and N_2 adsorption experiments.

2.3 Characterization methods: FTIR, PXRD, SEM, TGA, DSC and N_2 adsorption

Fourier transform infrared (FTIR) spectra were recorded on a Perkin Elmer Spectrum Two Fourier transform infrared spectrometer using the attenuated total reflectance (ATR) method with a diamond crystal [28, 29]. Spectra were obtained on powders without addition of KBr. X-ray diffraction patterns was recorded with a Bruker D8 Discover diffractometer (2θ values between 2 and 70°, Cu K_α radiation with a wavelength of 0.15406 nm on dried powders [28, 29]. For comparison, a simulated XRD pattern of HKUST-1 ($Cu_3(BTC)_2$) was produced using Winplot X.2 software from the CCDC web site (deposition number 112954) [16]. The morphological features of materials were examined by SEM on a Philips XL30-FEG scanning electron microscope. Particle size analysis was performed using Image J software. BET (Brunauer Emmett Teller) surface areas were determined using a Micrometrics ASAP-2420 instrument with N_2 at 77 K. Prior to measurements; the powders were outgassed for 24 h under vacuum at 423 K [28, 29]. The pore size distribution was determined using the Horvath-Kawazoe (H–K) model [28]. Thermogravimetric (TGA) analysis was carried out using a TG Mettler Toledo STARe apparatus under air from 298 K up to 973 K with a temperature ramp of 10 K/min. Differential scanning calorimetry (DSC) was performed using a Mettler-Toledo TGA/DSC 3+ [28, 29].

Table 1. MOFs and templated MOFs (Soft templ.) for CH_4 and CO_2 adsorption, the specific BET surface area (S_{BET}), the pore volume (V_p), the particle (Part.) size, and the pore diameter (diam).

Adsorbents	Soft templ.	S_{BET} m^2/g	V_p cm^3/g	Part. size nm	Pore diam. nm	CH_4 uptake $mg(CH_4)/g$	CO_2 uptake $mg(CO_2)/g$	Adsorption condition	Ref.
Al(OH)(ndc)-DUT-4[a]	None	1308	0.68	-	-	40	396	303 K, 10 bar	[31]
MIL-101(Fe)-NH_2	None	915	0.43	200-500	-	80	660	303 K, 10 bar	[32]
ZIF-68[b]	None	1090	-	-	1.03	7.2	61.6-79.2	298 K, 1 bar	[33]
ZIF-69[c]	None	950	-	-	0.78	7.2	61.6-79.2	298 K, 1 bar	[33]
ZIF-70[d]	None	1730	-	-	1.59	7.2	61.6-79.2	298 K, 1 bar	[33]
MOF-2[e]	None	378	-		-	20.8	224.4	298 K, 30 bar	[34]
$Cu(HBTB)_2$[f]	None	600	-		-	56	330	298 K, 25 bar	[35]
Cu-BTC[g]	None	1571	0.79	-	-	73.6	558.8	298 K, 15bar	[36]
Mg-MOF-74	None	1174	-	1000-2000	1.02	16	360.8	298 K, 1 bar	[37]

Cu-MOF	None	1450	0.50	500-1000	-	5.6	28.6	298 K, 1 bar	[38]
Zn-MOF-74	None	816	-	-	1.1	-	404.8	298 K, 42 bar	[39]
$Cu_3(BTC)_2$	None	1781	-	57	0.5/1.5	-	488.4	298 K, 42 bar	[39]
ZIF-8[h]	None	1502	0.54	90	0.7/1.05/1.2	-	469.9	298 K, 40 bar	[40]
ZIF-8	PDADMAC[i]	1264	0.51	57	-	-	347.6	298 K, 40 bar	[41]
ZIF-67[j]	None	1478	0.66	500-1000	0.64/0.9/1.04	-	513.9	298 K, 50 bar	[42]
Cu-BTC	None	1737	0.73	-	-	-	596.64	-	[43]
K/Cu-BTC	none	1188.6	0.52	$(10\text{-}20)\times10^3$	-	-	380.16	298 K, 18 bar	[44]
HKUST-1	none	1410	0.71	10-50	0.64	-	348.48	196 K, 1 bar	[45]
SWCNT@HKUST-1	SWCNT[k]	1714	0.9203	-	0.67	-	385	196 K, 1 bar	[45]
Zr-MOF	none	1433	0.63	63	0.88	57.6	356.4	273 K, 9.8 bar	[46]
Zr-MOF-NH_4	none	1320	0.61	41	0.93	44.8	343.2	273 K, 9.8 bar	[46]
MOF-199	none	1448	0.69	60-130 µm	1.18	-	405.54	298 K, 25.8 bar	[47]
n-ZIF-8	**PEG**[l] **20,000**	1694	0.67	60-260	0.787	211.58	547	298 K, 40 bar	[28]
n-ZIF-67	**PEG 20,000**	1891	0.86	30-100	0.64	241	681	298 K, 40 bar	[29]
HKUST-1	**PEG 20,000**	**1904**	**0.87**	**$100\text{-}1.2\times10^5$**	**0.84**	**214**	**708**	**298 K, 40 bar**	**This work**

[a] Al(OH)(ndc)-DUT-4 with ndc as 2,6-naphthalene dicarboxylate; [b] Zn(bIm)(nIm) with bIm as benzimidazole and nIm as 2-nitroimidazole; [c] Zn(cbIm)(nIm) with cbIm as 5-Chlorobenzimidazole; [d] $Zn(Im)_{1.13}(nIm)_{0.87}$ with Im as ditopic imidazolate; [e] $C_{29}H_{19}F_9NO_{8.25}Zn_2$; [f] $Cu(HBTB)_2$ with H_3BTB as 1,3,5-tris(4-carboxyphenyl) benzene) ; [g] Cu-BTC with BTC as 1,3,5-benzenetricarboxylic acid; [h] $Zn(mIm)_2$ with mIm as 2-methylimidazolate [i] PDADMAC as poly(diallyldimethylammonium chloride); [j] $Co(mIm)_2$;[k] SWCNT as single-walled carbon nanotubes ; [l] $PEG_{20,000}$ as polyethylene glycol with an average molecular weight of 20,000 g/mol.

2.4 Adsorption isotherms: CO_2, CH_4 and N_2

The adsorption isotherms of CO_2, CH_4 and N_2 on the PEG-templated HKUST-1 MOF were measured by gravimetric analysis (Autosorb-iQ-MP analyzer) in the pressure range of 0-40 bar, and at four temperatures varying from 273 to 353 K. Prior to the measurement, the powder was outgassed at 423 K for 24 h to desorb any air and moisture desorbed on the surface. The CO_2 and CH_4 gases were of high purity (99.99%) and obtained from Sigma-Aldrich. The thermodynamics parameters (ΔH°, ΔS° and ΔG°) [700] and isosteric heats of adsorption (Q_{st}) were calculated based on sorption isotherms measured up to 40 bar at 273, 298, 323 and 353 K. The isotherms were fitted with the Langmuir isotherm model [500]. The isosteric heats of adsorption were calculated by applying the Clausius-Clapeyron equation [800].

[700] S. Ullah, M. A. Bustam, M. A. Assiri, A. G. Al-Sehemi, G. Gonfa, A. Mukhtar, F. A. Abdul Kareem, M. Ayoub, S. Saqib, N.B. Mellon, Synthesis and characterization of mesoporous MOF UMCM-1 for CO2/CH4 adsorption; an experimental, isotherm modeling and thermodynamic study, Microporous Mesoporous Mater. 294 (2020) 109844.

[500] I. Langmuir, The adsorption of gases on plane surfaces of glass, mica and platinum. J Am. Chem. Soc. 40 (1917) 1361-1403.

[800] S. Builes, S. I. Sandler R. Xiong, Isosteric Heats of Gas and Liquid Adsorption, Langmuir. 29 (2013) 10416-10422.

2.5 Separation of gas mixtures: CO_2/N_2, CH_4/N_2 CO_2/CH_4

Breakthrough experiments were performed using a stainless steel column with a length of 10 cm and an internal diameter of 10 mm. The column was packed with 4.5 g of the adsorbent, PEG-templated HKUST-1, and was activated under helium flow [48]. Breakthrough curve measurements were carried out in two steps. Prior to flowing the feed gas into the adsorption column, the gas was bubbled in an equilibrium column for 10 min to achieve a stabilized and equilibrated system. Separation measurements were subsequently performed at 298 K and at atmospheric pressure. CO_2/N_2, CH_4/N_2 CO_2/CH_4 mixtures (50/50, v/v) were tested at flow rates of 15 and 30 mL/min. The gas stream was analyzed by gas chromatography at the outlet of the column.

3. Results and discussion

3.1 Physico-chemical characterization of PEG-templated HKUST-1 MOF

The structure of the new adsorbent was first characterized by FTIR. The FTIR spectrum of the new PEG-templated HKUST-1 is presented in Fig. 1 (a) alongside the spectrum of the ligand precursor. The first zone (fingerprint region) for PEG-templated HKUST-1 from 600 to 1300 cm^{-1} corresponds to the various vibration signals of the H_3BTC ligand. Particularly, the band at 1093 cm^{-1} is attributed to the C-O-Cu stretching mode of HKUST-1. The zone between 1300 and 1700 cm^{-1} is related to the carboxylate groups of the ligand and is thus indicative of the coordination of benzene-1,3,5-tricarboxylic acid (BTC) bridging ligands with copper nodes [100, 200]. The specific bands located at 1645, 1563, 1448 and 1377 cm^{-1} correspond to the asymmetric and symmetric stretching vibrations of the carboxylate groups of HKUST-1, respectively. The band at 490 cm^{-1} is related to the Cu-O stretching mode of the framework structure, further consistent with the successful isolation of a HKUST-1 MOF. The broad bands at 3400-3000 cm^{-1} corroborate the presence of humidity in the powders. The FTIR spectrum shows the typical bands of HKUST-1 MOF ($Cu_3(BTC)_2$) and is consistent with spectra reported elsewhere [49, 50].

[100] L. T. L. Nguyen, T. T. Nguyen, K. D. Nguyen, N. T. S. Phan, Metal–organic framework MOF-199 as an efficient heterogeneous catalyst for the aza-Michael reaction, Appl. Catal. A: Gen. 425 (2012) 44-52.

[200] A. Roy, A. K. Srivastava, B. Singh, D. Shah, T. H. Mahato, A. Srivastava, Kinetics of degradation of sulfur mustard and sarin simulants on HKUST-1 metal organic framework, Dalton. Trans. 41 (2012) 12346-12348.

Similar conclusions were drawn from the XRD measurements; the XRD pattern (Fig. 1 (b)) confirms that the PEG-templated corresponds well to the typical structure of HKUST-1 ($Cu_3(BTC)_2$) with a cubic structure (*Fm-3m*) [16]. The crystallite~~s~~ size was estimated based on the Debye-Scherrer equation (see Equation S1) and found to be about 107.69 nm. The particle size was also estimated using Scherrer's technique, and also the Williamson-Hall (W-H) method from a plot with sin (θ) along the x-axis and $\beta_{hkl}\cos(\theta)$ along the y-axis (Fig. 1 (c)). The slope and y-intersect of the fitted line relate to the particle size and the strain, respectively. The calculated crystallite size is 254.9 nm based on the W-H method and 107.7 nm based on Scherrer's technique. The larger estimated crystallite size for the W-H method is likely related to the impact of strain effects which also contribute to peak broadening.

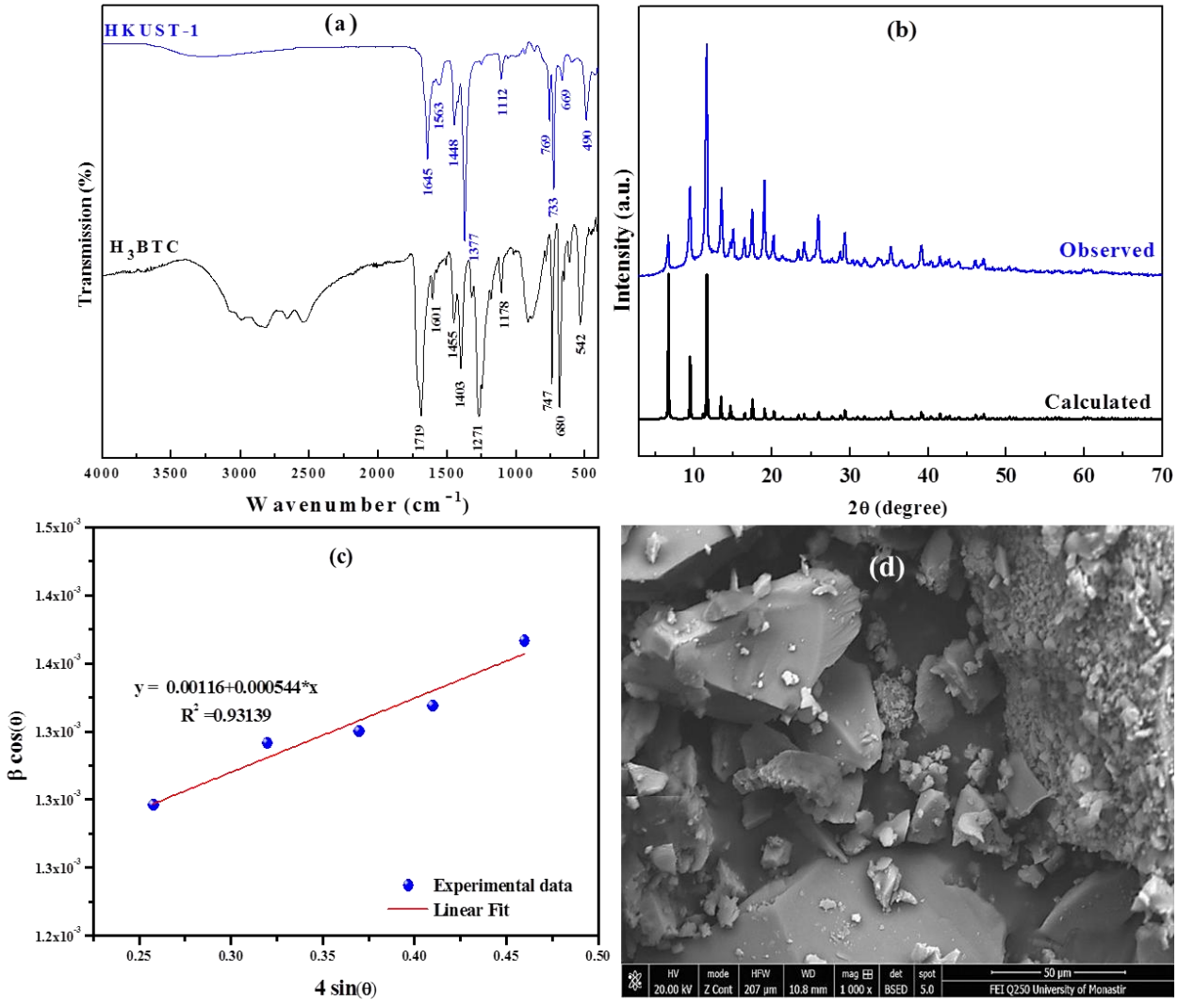

Fig. 1. (a) FTIR spectrum of the benzene-1,3,5-tricarboxylic acid (H_3BTC) ligand (black line) and the PEG-templated HKUST-1 MOF formed from Cu and H_3BTC (blue line); (b) ~~X-ray powder diffraction~~ PXRD patterns of our experimental sample (blue line) and

simulated HKUST-1 (~~from~~ CIF: ~~with reference~~ CCDC 112954) (black line); (c) Plot of β cosθ vs. 4 sinθ; (d) SEM micrograph of PEG-templated HKUST-1 at 1000× magnification.

The morphology of the HKUST-1 material was examined by SEM (Fig. 1 (d)). The micrograph~~s~~ display~~s~~ a large distribution of nano- and micro-particles with crystal surface features such as a regular smooth surface and faceted structure [49] with sizes ranging from 100 nm to 120 µm. HKUST-1 ($Cu_3(BTC)_2$) is conventionally obtained by solvothermal synthesis and typically gives microparticles of around 60 µm [51]. Thi et al. reported MOF-199 ($Cu_3(BTC)_2$) microparticles with crystal sizes ranging between 30 and 130 µm [47]. The PEG-templated synthesis therefore gives rise to the 'classical' microparticles but also provides easy access to a large nanoparticle size distribution; the latter ~~of which~~ are of high interest for gas adsorption and separation. The size of the nanoparticles corresponds well with the crystallite sizes obtained via the Scherrer and W-H techniques, importantly, highlighting the dominant presence of the nanoparticles.

The thermal stability and degradation of the HKUST-1 MOF was subsequently studied by TGA and DSC analysis (Fig. 2). The TGA curve for the HKUST-1 particles exhibits two stages of weights loss: the first weight loss of 23.15 % of the initial sample occurred between 303 to 433 K and corresponds to the removal of terminally-coordinated water molecules. This is supported by an exothermic signal peaking at 313 K. The second weight loss of 61.28% started at 573 K and continued to 650 ~~723~~ K, as evidenced by an exothermic peak maximum at 623 K. This second feature is mainly due to decomposition of the adsorbent. The PEG-templated HKUST-1 is therefore considered stable at temperatures up to 594 K. A lower temperature of 423 K was chosen as a suitable temperature for degassing prior to gas sorption experiments. The TGA and DSC results for the PEG-templated adsorbent correlate with those reported for the HKUST-1 synthesized by Thi et al. [47]. Finally, at 723 K only about 10.65 wt% of the starting weight remained. The thermal decomposition of HKUST-1 beyond this temperature gave rise to a black precipitate that may be assigned to copper oxides (e.g. CuO phase) in accordance with reported data in the literature [52].

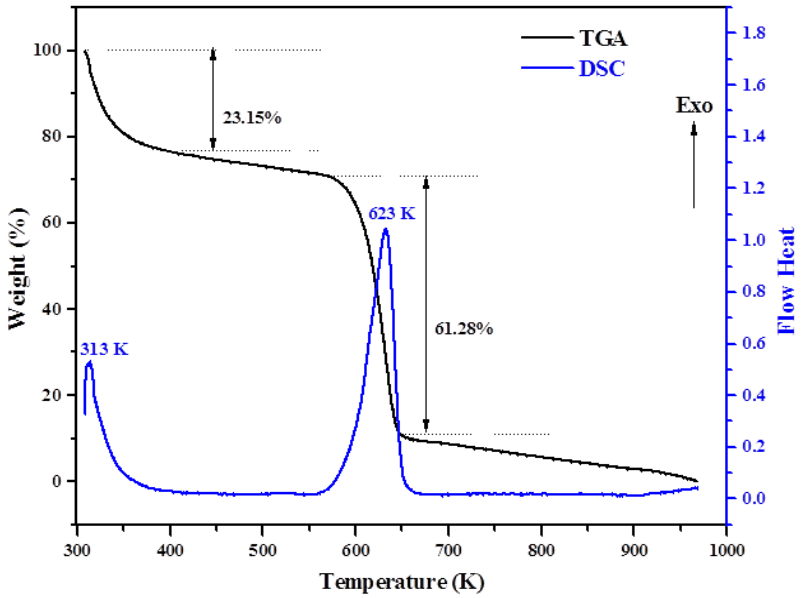

Fig. 2. TGA and DSC analyses of PEG-templated HKUST-1 under air and with a heating rate of 10°C/min.

Next we turned our attention to evaluating the porous structure of the PEG-templated HKUST-1 material. The blue powders were activated at 423 K under vacuum for 24 h prior to nitrogen gas sorption measurements. Nitrogen adsorption/desorption isotherms for PEG-templated HKUST-1 are shown in Fig. 3 (a). The adsorption equilibrium was reached quickly at the low relative pressure region (P/P° from 10^{-5} to 10^{-1}) while an adsorption plateau and no hysteresis loops were observed at large relative pressure. According to the International Union of Pure and Applied Chemistry (IUPAC) classification [53], this behaviour is consistent with a typical type I isotherm. Generally, such materials are characteristically microporous in nature (pore size < 2 nm) [54]. A maximum BET surface of 1904 m^2/g and total pore volume of 0.87 cm^3/g was determined for the microporous PEG-templated HKUST-1 based on N_2 adsorption at relative pressures of 0.04-0.3 and 0.9, respectively. A classical 24 hour solvothermal synthesis of MOF-199 (HKUST-1, $Cu_3(BTC)_2$) at 358 K from a DMF reaction mixture produced particles with a BET surface area of 1448 m^2/g, and 0.693 cm^3/g maximum pore volume [47]. The BET surface area and porous volume of PEG-templated HKUST-1 are also much higher than values for $Cu_3(BTC)_2$/HKUST-1 of 692 m^2/g and 0.33 cm^3/g, 1482 m^2/g and 0.753 cm^3/g, and 1296 m^2/g and 0.69 cm^3/g reported by Chui et al., Li and Yang, and Chowdhury et al. [16, 55, 56].

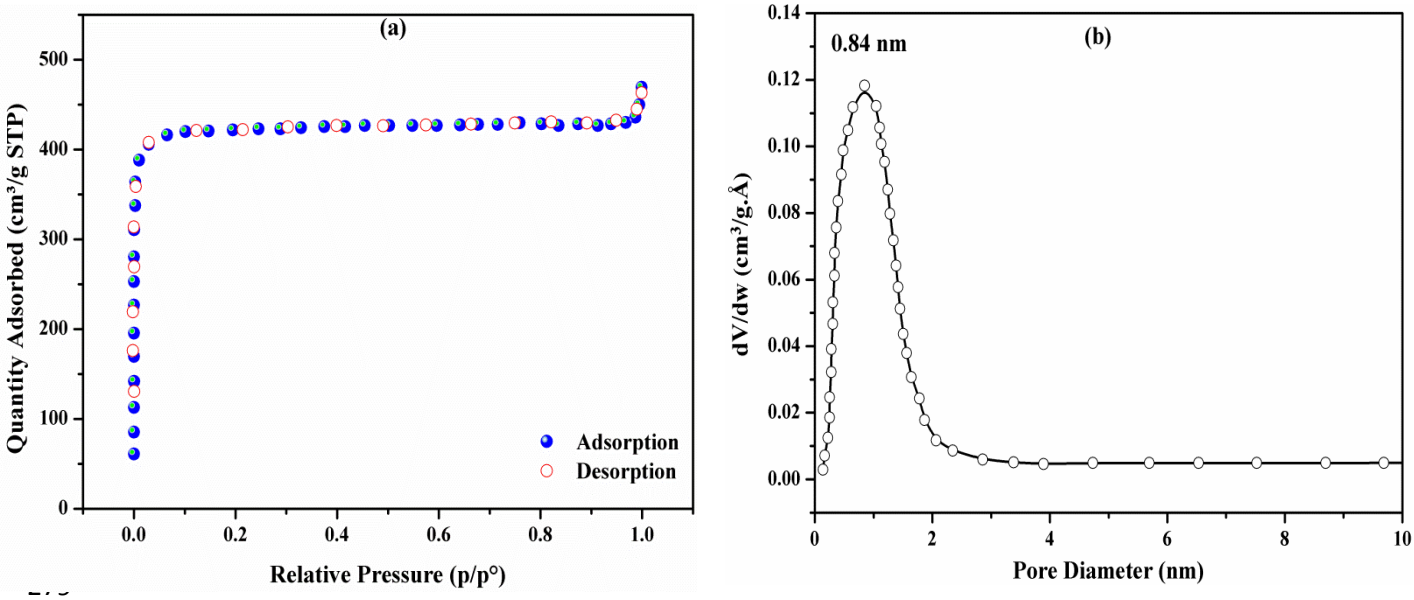

Fig. 3. (a) N_2 adsorption-desorption isotherms of PEG-templated HKUST-1 and (b) corresponding pore size distribution.

These porosity values are unusually high and certainly attractive when compared with the published results for reported HKUST-1($Cu_3(BTC)_2$) particles and other highly porous MOFs (Table S1). We note that the unusually high surface area is consistent with effective removal of the PEG template but that the possibility that some residual PEG remains is not completely ruled out [57-59].

The pore size distributions (Fig. 3 (b)) shows one peak centered at 0.84 nm, confirming the microporous structure of PEG-templated HKUST-1. In the previous study by Thi et al, the synthesized MOF-199 with mean pore size of 1.18 nm was demonstrated as an effective stable and rigid adsorbent for CO_2, for example, exhibiting a storage capacity of 9.21 mmol/g at a pressure of 25.76 bar with almost reversible adsorption/desorption isotherms [47]. The comparatively smaller pores of the PEG-templated HKUST-1 combined with the large overall BET surface area are therefore promising.

3.2 Gas adsorption studies at PEG-templated HKUST-1: CO_2, CH_4 and N_2

We subsequently investigated the capacity of the new adsorbent for CO_2, CH_4 and N_2 capture and storage at different temperatures from a low to high pressure range of 0 to 40 bar. First, we considered the adsorption of CO_2 and CH_4. Fig. 4 (a) reveals that the adsorption of CO_2 increases with increasing pressure, reaching equilibrium (adsorption plateau) at higher temperatures and at all pressures. This behaviour is consistent with a strong adsorption capacity for CO_2. In contrast, the adsorption of CH_4, while also non-linear, increases more linearly with increasing pressure but no equilibrium is reached

regardless of the pressure and temperatures. This phenomenon is consistent with a weak interaction between CH_4 and the PEG-templated HKUST-1 MOF (Fig. 4 (c)). The adsorption isotherms for CO_2 and CH_4 that do not exhibit hysteresis are consistent with type I isotherms according to the IUPAC classification [53].

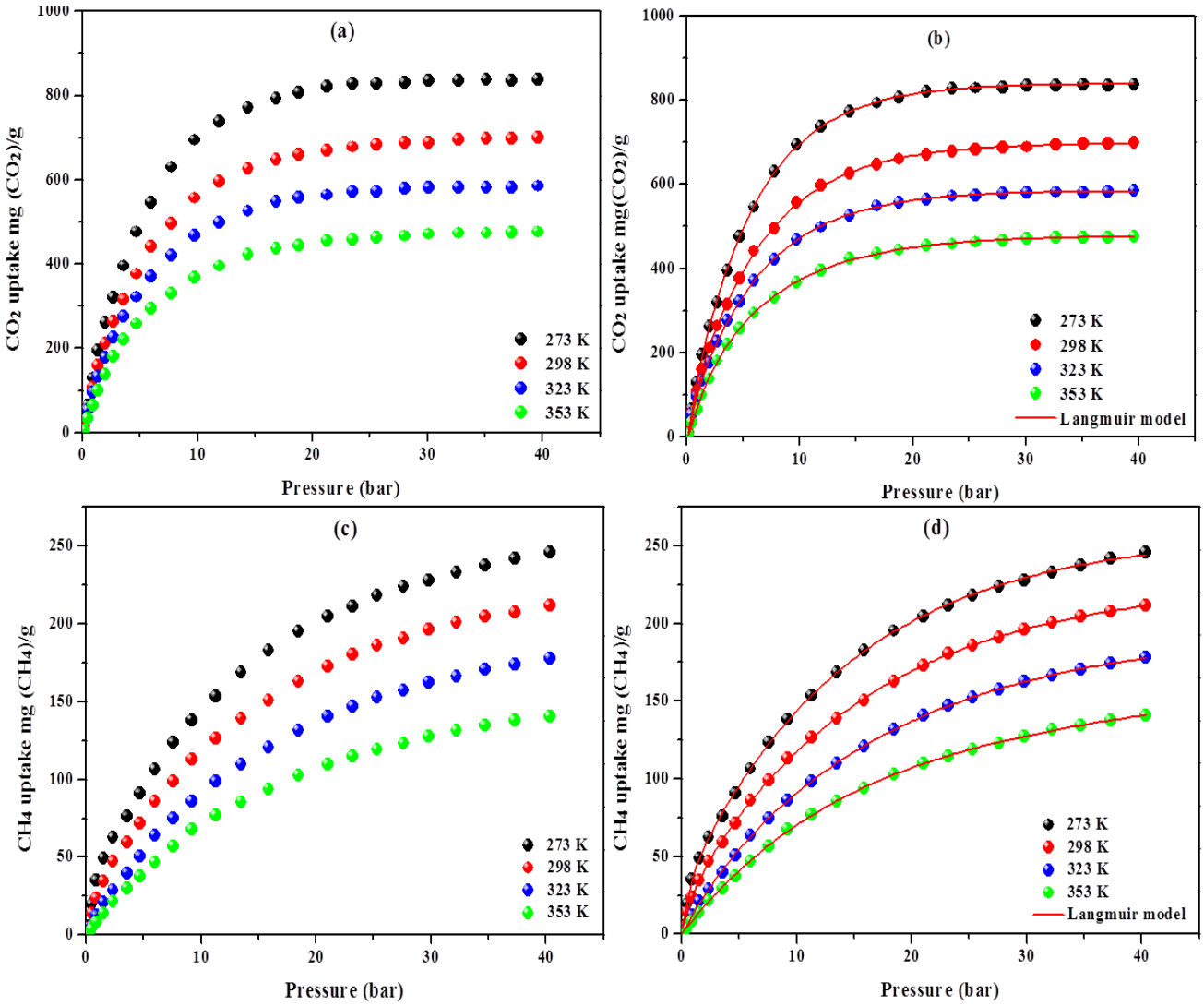

Fig. 4. (a) CO_2 adsorption isotherms at HKUST-1 MOF at high pressure (1-40 bar) and at 273, 298, 323 and 353 K; (b) the CO_2 adsorption isotherm fitted to the kinetic Langmuir model, (c) CH_4 adsorption isotherms recorded at PEG-templated HKUST-1 MOF at high pressure (1-40 bar) and at 273, 298, 323 and 353 K; (d) the CH_4 adsorption isotherm fitted to the kinetic Langmuir model.

For both CO_2 and CH_4, the adsorption capacity decreased with increasing temperature, revealing exothermic adsorption reactions [60]. The maximum adsorbed quantity of CO_2 is 708 mg (CO_2)/g (16.09 mmol/g) at 298 K and 40 bar, which is significantly higher than the adsorption capacity of many state-of-the-art MOF adsorbents (Table S1). Furthermore, we

emphasize that PEG-templated HKUST-1 shows a higher CO_2 adsorption capacity compared to our previous MOFs prepared using PEG as a soft template; namely, ZIF-8 [28] and ZIF-67 [29]. The superior results reported here for HKUST-1 can be linked, at least in part, to the unsaturated open Cu metal sites combined with the attractive pore characteristics including the very high specific surface area [61]. The maximum adsorbed quantity of CH_4 is much lower compared to CO_2 (214 mg(CH_4)/g at 298 K and 40 bar).

Adsorption isotherms for N_2 gas at HKUST-1 were also recorded and show increased adsorption with increasing pressure in the considered pressure range (Fig. 5 (a)). The maximum N_2 adsorption uptake was determined as 177.22 mg (N_2)/g (6.32 mmol/g) at 298 K and 40 bar. Lower levels of N_2 were adsorbed at higher temperatures (122.35 mg(N_2)/g at 353 K, for example). The increase in the equilibrium adsorption temperature that leads to a reduction in the amount of adsorbed N_2 is in agreement with an exothermic adsorption reaction, as was the case for CO_2 adsorption.

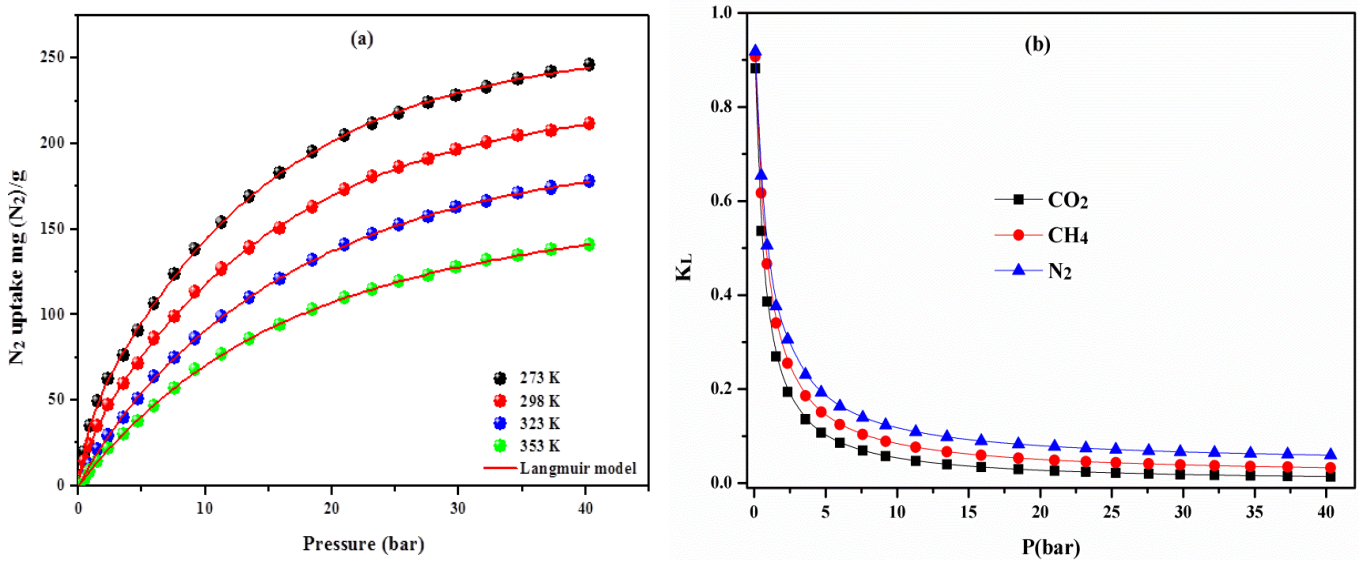

Fig. 5. (a) N_2 adsorption isotherms on PEG-templated HKUST-1 MOF with Langmuir model fitting and (b) Separation factor, R_L, plot vs. pressure for the adsorption of CO_2, CH_4 and N_2.

The PEG-templated HKUST-1 adsorbent exhibits a much higher CO_2 adsorption capacity compared to CH_4 and N_2. CO_2 has a greater quadrupole moment (13.4×10^{-40} C.m^2) compared to N_2 (4.7×10^{-40} C.m^2) that typically leads to a stronger interaction at the surface of adsorbents through physisorption processes, for example, involving polar adsorbent sites [62-64]. CH_4 has no dipole (nonpolar molecule) or quadrupole moment hence adsorption is not simply based on moment-surface interactions [65]. The higher CO_2 adsorption capacity can be partially supported by favorable electrostatic interactions between unsaturated Cu^{2+}

and axially aligned CO_2 quadrupole moments with negatively-charged oxygen [61, 66, 67]. Other factors to consider include the similar sizes of the molecules as well as their different polarizabilities where CO_2 and CH_4 are more polarizable than N_2 (26.3×10^{-25} vs. 17.6×10^{-25} vs. 26.0×10^{-25} cm^3 for CO_2, N_2, and CH_4, respectively) [68].

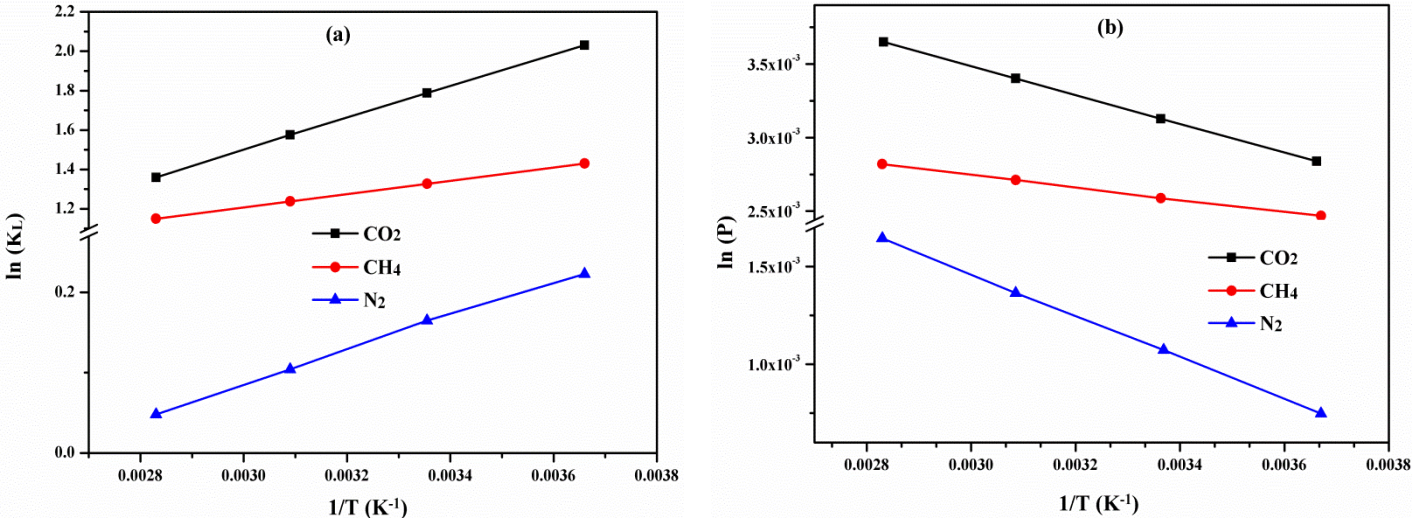

Fig. 6. Evolution of (a) ln (k_L) as a function of 1/T and (b) ln (P) as a function of 1/T for CO_2, CH_4, and N_2.

We performed further analysis on the gas adsorption isotherm data to shed new light on the PEG-templated HKUST-1 adsorbent properties. Fig. 4 and Fig. 5 show the CO_2 CH_4, and N_2 adsorption isotherms fitted according to the Langmuir model (R^2 of ca. 0.99). The Langmuir kinetic model gave the best fitting with the experimental data for CO_2 and CH_4. The estimated physical parameters and correlation coefficients are summarized in Table S2. With reference to the Langmuir model, the equilibrium adsorption capacity, q_m, and the adsorption equilibrium constant, K_L, of PEG-templated HKUST-1 were determined for the three gases (Table S2). In all cases, the equilibrium values were found to decrease with increasing temperature, consistent with physical rather than chemical gas adsorption at the adsorbent surface [28, 29, 69].

3.3 Thermodynamic investigations of PEG-templated HKUST-1

To gain further understanding of CO_2, CH_4 and N_2 adsorption at PEG-templated HKUST-1, we investigated several thermodynamic parameters (see ~~ESI~~ Supporting Information for equations and calculation details). The Gibbs free energy (ΔG°), standard enthalpy (ΔH°) and standard entropy (ΔS°) were calculated and are summarized below in Table 2. For all three gases, the negative values of ΔG° highlight the spontaneity and feasibility of the gas adsorption process at all temperatures studied. The values of ΔG° decreased with

increasing temperature, revealing that the adsorption processes are more feasible at lower temperatures and especially for CO_2. The ΔG° values were in all cases between -2.77 and -0.53 kJ/mol, indicating physical adsorption (0 to -20 kJ/mol) rather than chemisorption (-80 to -400 kJ/mol) for the three gases at the PEG-templated HKUST-1 surface [70].

Table 2 Thermodynamic properties for CO_2, CH_4 and N_2 adsorption at PEG-templated HKUST-1.

	ΔH°(kJ/mol)	ΔS°(J/K)	ΔG° (kJ/mol)			
			273 K	298 K	323 K	353 K
CO_2	-6.52±	-13.72±	-2.77±	-2.43±	-2.08±	-1.67±
CH_4	-4.93±	-11.38±	-1.82±	-1.53±	-1.25±	-0.91±
N_2	-3.76±	-9.13±	-1.26±	-1.03±	-0.81±	-0.53±

The linear Van't Hoff plot of ln (K_L) vs 1/T that relates the change in temperature to the change in equilibrium constant was used to obtain the standard enthalpy and entropy change from the slope and the intercept, as presented in Fig. 6 (a). The negative values for ΔH° are between -3.76 and -6.52 kJ/mol, that is, in the 0 to -20 kJ/mol ranges, further highlighting the exothermic nature of the physical adsorption process for each of the three gases [70]. The slightly larger negative enthalpy for CO_2 adsorption is consistent with a stronger adsorption interaction albeit through apparently weak bonding interactions. The negative standard entropy changes suggest that the magnitude of the randomness of the gases became more ordered (decreased) during the physical adsorption processes, consistent with the transition of the molecules in the random gaseous state to an organized solid-like phase at PEG-templated HKUST-1.

An important parameter to provide a deeper insight into the adsorption process of gases at MOFs and other porous materials is the heat (or enthalpy) of adsorption. The isosteric heat of adsorption (Q_{st}) measures the change of enthalpy when gas adsorbate molecules are adsorbed from the bulk phase to the adsorbed phase, providing insight into the binding affinity of adsorbed molecules for surface sites on the absorbent. Here we calculated the pure component isosteric heat of adsorption via the Clausius-Clapeyron equation and pure adsorption isotherm data recorded in the range 273-353 K for CO_2, CH_4, and N_2. The Q_{st} values were obtained after plotting the logarithm of the pressure as a function of the reverse of the temperature (Fig. 6 (b)). The slope of the plots is negative due to the exothermic nature of the adsorption processes.

The isosteric heats for CO_2, CH_4 and N_2 adsorption (Q_{st}) were calculated from the Langmuir-fitted experimental isotherm data recorded at the range 273-353 K at PEG-templated HKUST-1, and are presented in Fig. 7 (a). First, we observe that the isosteric heat of adsorption decreases slightly with increasing loading of adsorbed gas molecules, attributed to heterogeneity in the adsorbent, especially during the initial loading phase, and especially for CO_2 adsorption. The Q_{st} values for CO_2 of 27.5 to 30.5 kJ/mol at 273-353 K were the highest observed and more than double the values observed for N_2 adsorption. The values of Q_{st} > 10 kJ/mol highlight a practical affinity for the gases and especially for CO_2 adsorption at PEG-templated HKUST-1. The Q_{st} that reflects the bond strength of the adsorbent-adsorbate interaction is the highest at lower coverages, reflecting the presence of a limited number of initial sites with higher affinity for the initial gas molecules [71, 72]. The affinity nevertheless remains high for CO_2 even after 5-15 mg/g adsorption. The higher thermodynamic affinity of CO_2 for PEG-templated HKUST-1 can be at least partially explained by the presence of strong quadrupolar interactions of CO_2 with the micropores of the adsorbent including specific interactions with coordinatively unsaturated copper sites (Cu^{2+}) [61, 66, 67]. The heat of CO_2 adsorption at PEG-templated HKUST-1 is higher than many values reported in the literature for synthesized HKUST-1 (Cu-BTC, $Cu_3(BTC)_2$) particles [73-75]. Pepe et al. measured 25.9 kJ/mol at Cu-BTC [72], while Wang et al. and Moellmer et al. measured 25 kJ/mol [74] and 29.2 kJ/mol [75], respectively. The values are lower than the heat of adsorption reported for CO_2 with the commercially-available CO_2 adsorbent, zeolite 13X (49 kJ/mol) [76]. A lower isosteric heat of adsorption has the upside that there is a reduced energy requirement for the desorption and therefore regeneration of the adsorbent.

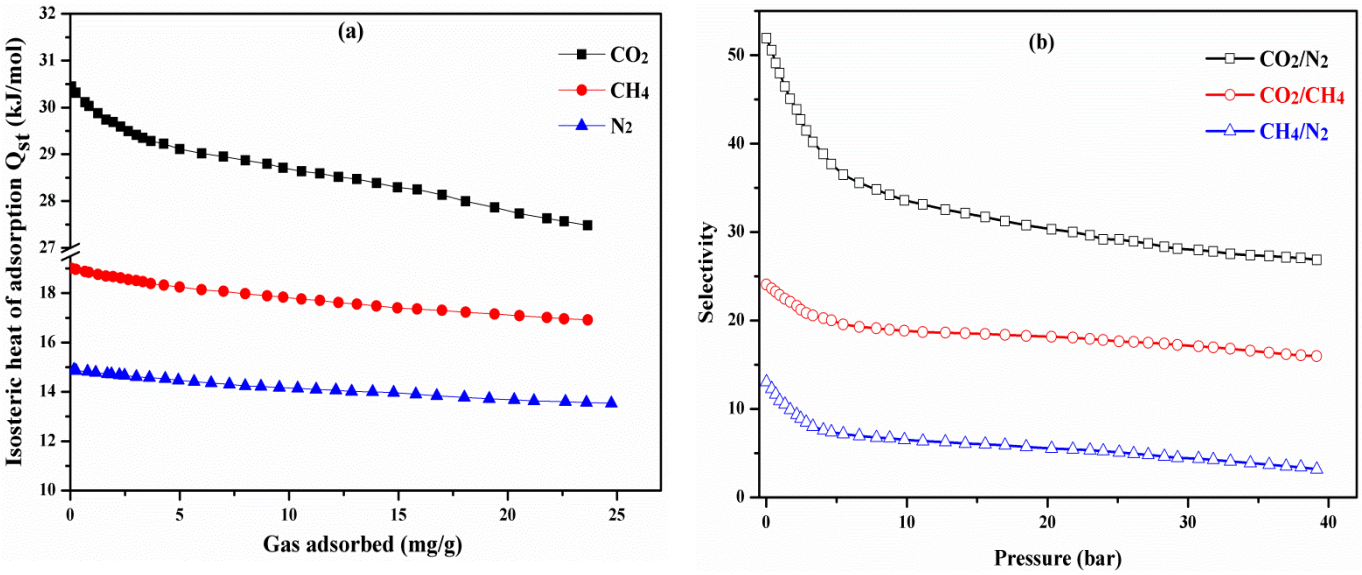

Fig. 7. (a) Isosteric heats of adsorption, Q_{st}, for CO_2, CH_4, and N_2 at PEG-templated HKUST-1 at 273-353 K (b) CO_2/N_2 and CO_2/CH_4 selectivities of PEG-templated HKUST-1 at 298 K.

A noteworthy high affinity of PEG-templated HKUST-1 for CH_4 was observed. A value of ca. 19 kJ/mol indicates strong binding between polarizable CH_4 molecules and the surface sites of the adsorbent. Both CO_2 and CH_4 adsorption energies are higher than those reported for commercially-available activated carbon e.g. 16-25 kJ/mol for CO_2 and 16-20 kJ/mol for CH_4, respectively [77]. Fig. 7 (a) shows that the isosteric heat of adsorption values for N_2 are notably smaller than for CH_4 and CO_2, and that the change in the heat of adsorption with gas surface coverage is very low. In other words, the N_2-adsorbent interaction remains heterogeneous but is much more homogeneous in nature compared to the CO_2–adsorbent adsorption. The isosteric heat of adsorption for N_2 uptake was equal to 14.90 kJ/mol, which is higher than values reported elsewhere [78, 79]. The lower thermodynamic affinities for CH_4 and N_2 bode well for the favorable potential selectivity of the PEG-templated HKUST-1 material for CO_2/CH_4 and CO_2/N_2 separations, respectively.

3.4 Adsorption selectivity for binary gas mixtures: CO_2/N_2, CO_2/CH_4 and CH_4/N_2

Building on the preferential heats of adsorption for CO_2 compared to CH_4 and N_2 at the PEG-templated HKUST-1, we evaluated the gas selectivity of the adsorbent. The selectivity was estimated from single gas isotherms after dividing the adsorption capacity for CO_2 (or CH_4) by that of N_2 or CH_4 at each pressure point at 298 K [80]. The gas selectivity values at different pressures are shown by the plots in Fig. 7 (b) for CO_2/N_2, CO_2/CH_4 and CH_4/N_2. For all mixtures, the selectivity decreased with increasing pressure while the best selectivity was observed in the 0.01 to 5 bar range. The PEG-templated HKUST-1 shows superior selectivity for CO_2 separation from a CO_2/N_2 mixture, particularly at low pressure. The selectivity values of 52, 30, and 27 at 0.01, 20 and 40 bar are notably higher than those of previously reported HKUST-1 ($Cu_3(BTC)_2$) [80]. The CO_2/N_2 selectivity of PEG-templated HKUST-1 is higher than that of our previously-reported ZIF-67 (28.02) [29], and ZIF-8 (23.36) prepared via PEG templating methods [28]. At low pressure and at 298 K, the selectivity of HKUST-1 for CO_2/CH_4 is between 16 and 24 while the selectivity for CH_4/N_2 is between 3 and 13. These values are almost as high as the separations previously reported at Cu-BTC (HKUST-1) [80]. Eventually, at high pressure and at 298 K, the PEG-templated HKUST-1 becomes largely ineffective for

CH_4/N_2 separation with a separation selectivity of close to 1. The PEG-templated HKUST-1 MOF that can be synthesized rapidly therefore shows good promise for separating binary CO_2 gas mixtures.

3.5 Dynamic breakthrough experiments and cyclic stability for gas mixtures: CO_2/N_2, CO_2/CH_4 and N_2/CH_4

To further confirm the separation performance of PEG-templated HKUST-1 for CO_2/N_2, CO_2/CH_4 and N_2/CH_4 mixtures, real-time dynamic breakthrough experiments were carried out at 298 K and 1 bar. CO_2/CH_4 (50/50, v/v), CO_2/N_2 (50/50, v/v) and N_2/CH_4 (50/50, v/v) mixtures were flowed into a defined bed comprising the HKUST-1 adsorbent, as described in the Experimental Section. The breakthrough profiles at 15 and 30 mL/min are shown in Fig. 8. The data clearly reveals that the N_2 and CH_4 gases were initially eluted (breakthrough) and reached saturation in the first few min, while the CO_2 was selectively adsorbed until 8-13 min, depending on the flow rate. For the CO_2/N_2 mixture at 15 mL/min, the CO_2 breakthrough time was 14.70 min while the N_2 breakthrough time was just 1.87 min. The data clearly shows the preferential adsorption of CO_2 over N_2 or CH_4 and that the PEG-templated HKUST-1 is capable of completely separating CO_2/N_2 (50/50, v/v) and CO_2/CH_4 (50/50, v/v) mixtures with only a small amount of N_2 or CH_4 adsorption. The difference in breakthrough time is higher between CO_2/N_2 and both CO_2/CH_4 and CH_4/N_2 at both flow rates. The breakthrough times shortened and the separation capacity decreased in all cases as the feed gas rate increased. The breakthrough experiments are in accordance with the results reported in Fig. 8 (b). For the N_2/CH_4 separation, N_2 broke through the adsorption column first, supporting the notion that N_2 was adsorbed the least linked to its lighter nature and weaker interactions with the adsorbent. The weaker interaction is consistent with the weaker quadruple moment compared to CO_2, and weaker polarizability compared to both CO_2 and CH_4. For N_2/CH_4 separation at 15 mL/min, the breakthrough time of CH_4 was 6.72 min while that of N_2 was 3.12 min. The differences in breakthrough times are consistent with distinctively strong interactions between CO_2 molecules linked to both the pores and the unsaturated open Cu sites of PEG-templated HKUST-1 [66, 67, 78].

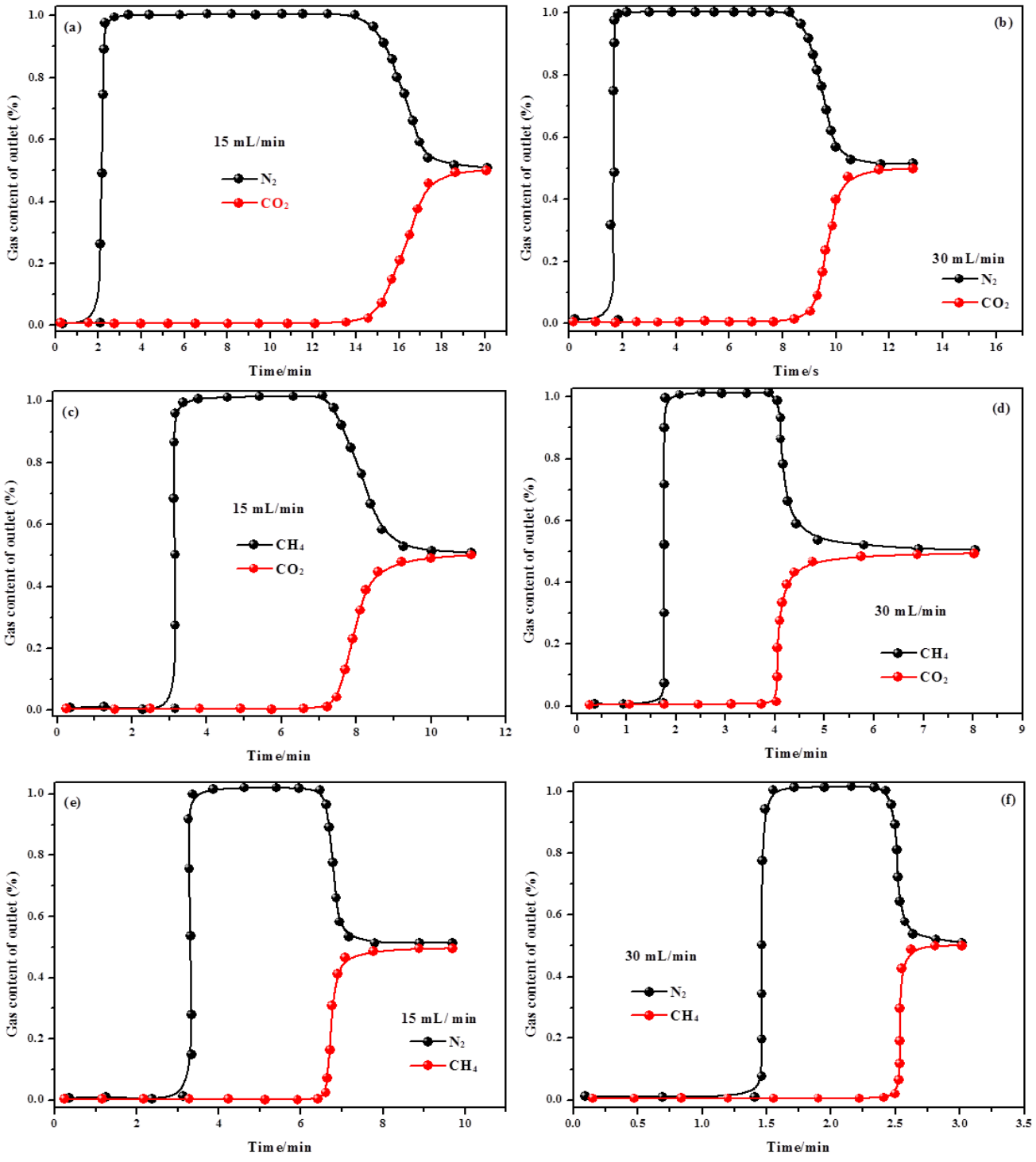

475

476 **Fig. 8.** Experimental breakthrough separation curves for equimolar mixtures of (a, b)
477 CO_2/N_2, (c, d) CO_2/CH_4, and (e, f) CH_4/N_2 at 1 bar and 298 K at different flow rates at
478 PEG-templated HKUST-1.

479 The reusability of adsorbents is crucial since it is linked to various ecological and
480 economical benefits, for example, including the mitigation of adverse environmental
481 impact [81]. We tested the reusability of the PEG-templated HKUST-1 by recording

multiple cycles of breakthrough experiments at 15 mL/min at 298 K. The breakthrough curves for the three gas mixtures showing 5-cycle reusability are shown in Fig. 9. There is no discernable change for the three gases, indicating outstanding cycle stability for the PEG-templated HKUST-1 adsorbent linked to the intrinsic stability of the MOF as well as the favorable and relatively low isosteric heat of adsorption. The desorption curve at 298 K shows that CO_2 completed desorbed after 14.70 minutes of helium purging.

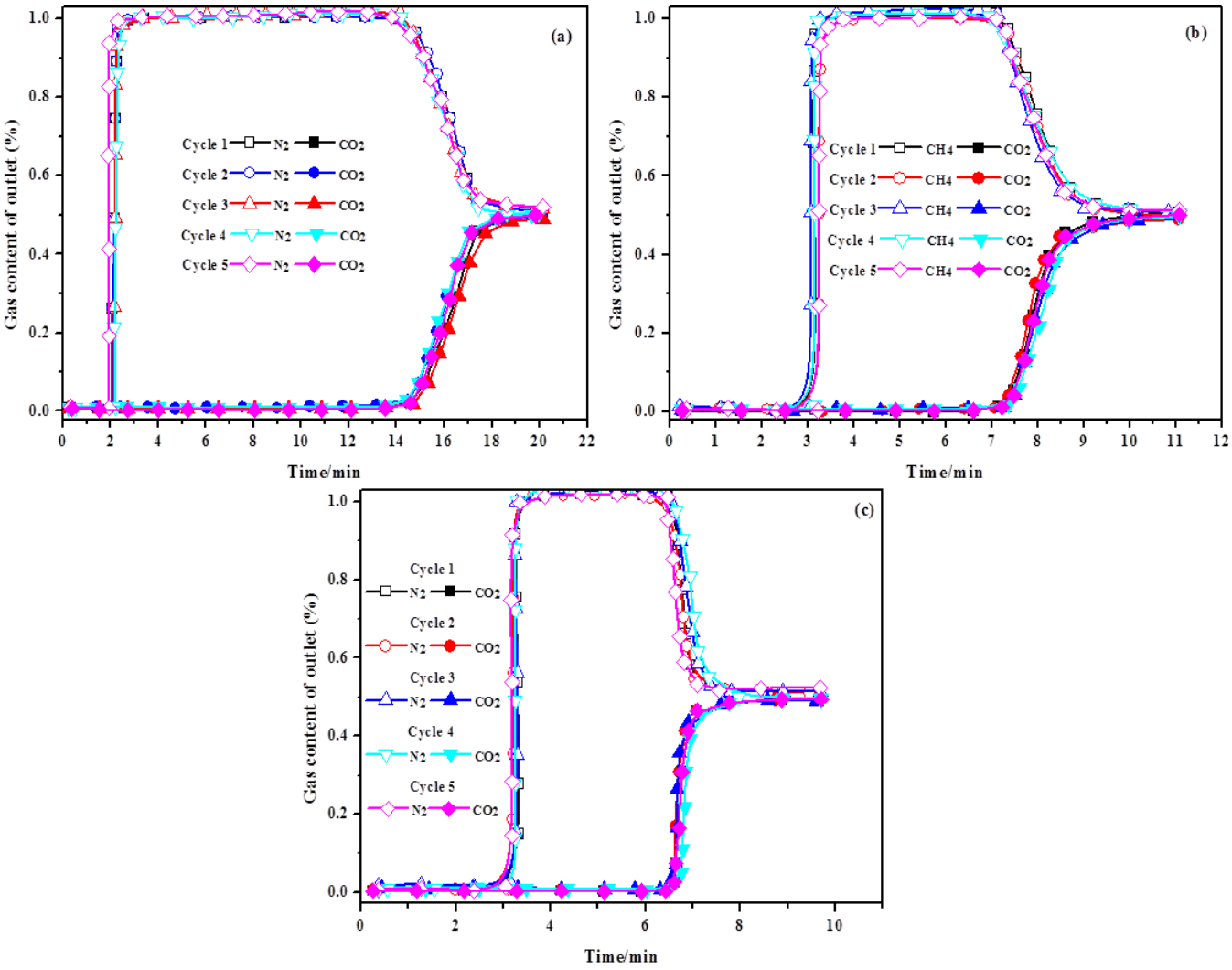

Fig. 9. Five breakthrough curve cycles for binary mixtures of (a) CO_2/N_2 (50/50, v/v), (b) CO_2/CH_4 (50/50, v/v), and (c) N_2/CH_4 (50/50, v/v), with helium gas purging, for PEG-templated HKUST-1 at 298 K.

3.6 Thermal adsorption/desorption stability evaluation

We finally made a more rigorous evaluation of the adsorption-desorption stability by performing prolonged CO_2 and CH_4 adsorption-regeneration cycles (5 cycles) using the pure gases (not mixtures). Following each adsorption cycle at 40 bar, the adsorbent was

heated to 393 K (10°C/min) under N_2 gas at 40 mL/min to desorb any adsorbed gases that remained on the surface of the adsorbent. The adsorbent was subsequently cooled to 298 K under N_2 and then weighed to complete a cycle. The percentage ratio of the adsorption capacity of the regenerated adsorbent to the initial adsorbent is defined as the adsorption index (AI) and is determined by the equation as follows:

$$AI = \frac{q_n}{q_1} \times 100 \qquad \text{Eq. (1)}$$

Where, q_1 and q_n indicate the CO_2 and CH_4 adsorption capacity for the first cycle and the n^{th} (n = 1-5) cycle, respectively. The adsorption-desorption stability can also be considered as a test of recyclability. The stability data for CO_2 and CH_4 adsorption at PEG-templated HKUST-1 at 298 K and 40 bar for 5 cycles each is shown in Fig. 10. The adsorbed amounts after 5 cycles of 708 mg(CO_2)/g and 214 mg(CH_4)/mg represent a loss of about 0.71 % and 0.97 %, respectively, compared to the initial adsorption capacity. The data confirms the robust and reversible or reusable nature of the adsorbent.

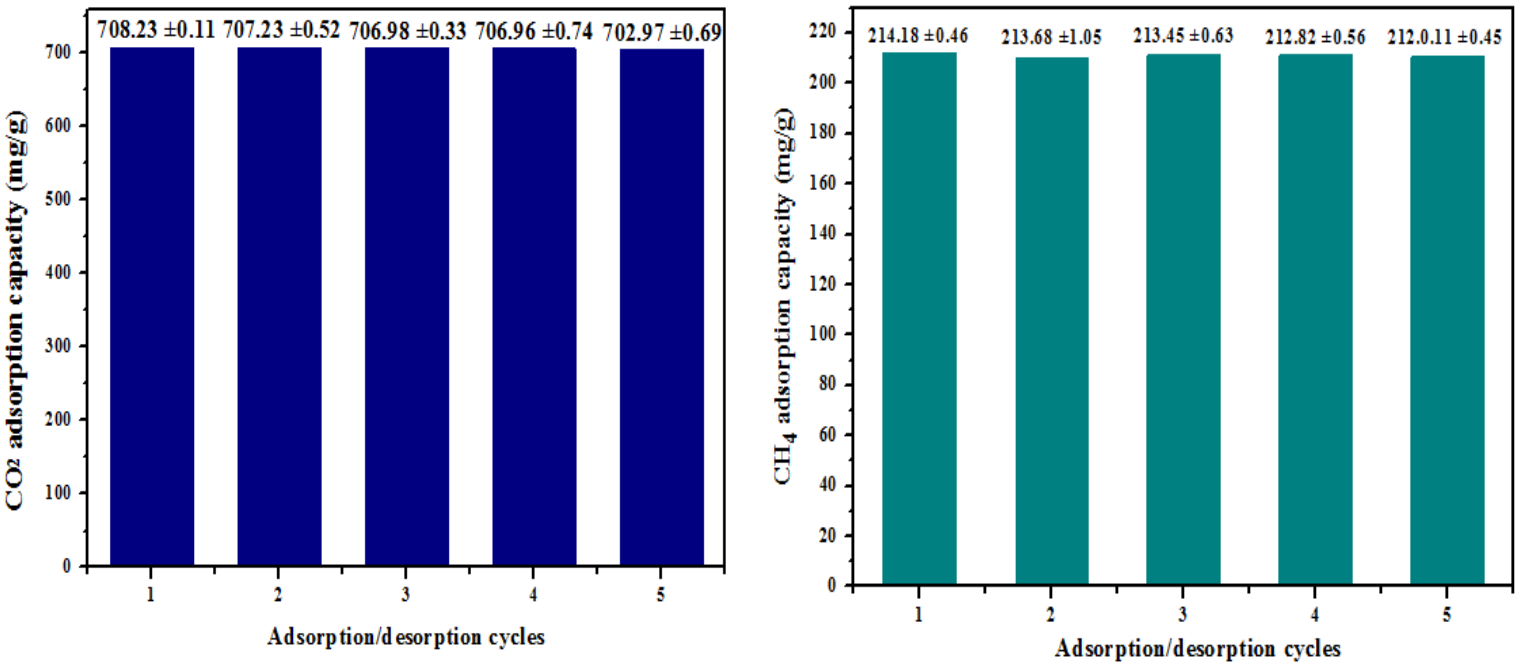

Fig. 10. Evolution of the CO_2 and CH_4 adsorption capacity of PEG-templated HKUST-1 over five adsorption/desorption cycles at 298 K and 40 bar.

4. Conclusion

We present a straightforward and rapid synthesis method for creating a highly microporous PEG-templated HKUST-1 MOF adsorbent with outstanding properties. The synthesized adsorbent exhibits a high N2 BET surface area of 1904 m2 /g and a mean pore volume of 0.87 cm3 /g, with attractive nanoparticle sizes (ca. 0.1–0.5 µm) alongside large microscale crystals (up to 120 µm). Gas adsorption studies demonstrate exceptional adsorption

capacities for CO2 and CH4 (708 mg (CO2)/g and 214 mg (CH4)/g, respectively, at 298 K and 40 bar), the highest reported for HKUST-1 (Cu-BTC) samples. The adsorption as well as separation performance is attributed to the high surface area and attractive microporosity as well as favorable surface interactions with physical rather than chemical interactions observed for all gases. Notably, CO2 adsorption interactions are linked to polar adsorbent sites, such as electrostatic interactions between unsaturated Cu2+ and aligned CO2 quadrupole moments with negatively charged oxygen. The adsorbent demonstrates practical and efective separation capacity for binary mixtures of CO2/N2 and CO2/CH4 in the 0.01 to 5 bar range, validated through breakthrough experiments. Excellent 5-cycle reusability data, with <1% performance loss, highlights the adsorbent's robustness and potential for economical production. Future research directions should focus on enhancing separation performance from ternary and more complex mixtures and gaining further insights into the polymer templating mechanism to develop new adsorbents with attractive porous architectures.

Funding: This research work was funded by the Institutional fund Projects under Grant No. IFPIP: 1241-155-1443.

Acknowledgements

The authors gratefully acknowledge technical and financial support provided by the Ministry of Education and King Abdulaziz University, DSR, Jeddah, Saudi Arabia, the ANR under reference ANR-20-CE05-0006, and PHC Utique Campus France programme (50221XB, CMCU 24G1208

References

[1] S. Pacala, R. Socolow, Stabilization wedges: solving the climate problem for the next 50 years with current technologies, Science. 305 (2004) 968-972.

[2] T. J. Crowley, Causes of climate change over the past 1000 years, Science. 289 (2000) 270-277.

[3] B. Metz, O. Davidson, H. C. D. Coninck, M. Loos, L. Meyer, IPCC special report on carbon dioxide capture and storage, Cambridge: Cambridge University Press, 2005.

[4] Y.S. Bae, R. Q. Snurr, Development and evaluation of porous materials for carbon dioxide separation and capture, Angew. Chem., Int. Ed. 50 (2011) 11586-11596.

[5] R.V. Siriwardane, M. S. Shen, E. P. Fisher, Adsorption of CO2, N2, and O2 on natural zeolites, Energy Fuels. 17 (2003) 571–576.

[6] B. Guo, L. Chang, K. Xie, Adsorption of carbon dioxide on activated carbon, J. Nat. Gas. Chem. 15 (2006) 223-229.

[7] S. Choi, J. H. Drese, C. W. Jones, Adsorbent materials for carbon dioxide capture from large anthropogenic point sources, Chem. Sus. Chem. 2 (2009) 796-854.

[8] Z. Zhang, Y. Zhao, Q. Gong, Z. Li, J. Li, MOFs for CO2 capture and separation from flue gas mixtures: the effect of multifunctional sites on their adsorption capacity and selectivity, Chem. Commun. 49 (2013) 653.

[9] G. Férey, C. M. Draznieks, C. Serre, F. Millange, Crystallized frameworks with giant pores: are there limits to the possible?, Acc. Chem. Res. 38 (2005) 217-225.

[10] D. Britt, D. Tranchemontagne, O. M. Yaghi, Metal-organic frameworks with high capacity and selectivity for harmful gases, Proc. Natl. Acad. Sci. 105 (2008) 11623-11627.

[11] S. L James, Metal-organic frameworks, Chem. Soc. Rev. 32 (2003) 276-288.

[12] J. S. Seo, D. Whang, H. Lee, S. I. Jun, J. Oh, Y. J. Jeon, K. Kim, A homochiral metal–organic porous material for enantioselective separation and catalysis, Nature. 404 (2000) 982-986.

[13] J. R. Li, R. J. Kuppler, H. C. Zhou, Selective gas adsorption and separation in metal–organic frameworks, Chem. Soc. Rev. 38 (2009) 1477-1504.

[14] Y. Cui, Y. Yue, G. Qian, B. Chen, Luminescent functional metal–organic frameworks, Chemi. Rev. 112 (2011) 1126-1162.

[15] J. H. Cavka, C. A. Grande, G. Mondino, R. Blom, High pressure adsorption of CO2 and CH4 on Zr-MOFs, Ind. Eng. Chem. 53 (2014) 15500-15507.

[16] S. S. Y. Chui, S. M. F. Lo, J. P. Charmant, A. G. Orpen, I. D. Williams, A chemically functionalizable nanoporous material [Cu3(TMA)2(H2O)3]n, Science. 283 (1999) 1148-1150.

[17] A. Vishnyakov, P.I. Ravikovitch, A.V. Neimark, M. Bülow, Q.M. Wang, Nanopore structure and sorption properties of Cu-BTC Metal−Organic framework, Nano. Lett. 3 (2003) 713-718.

[18] F. A. Kloutse, W. Gauthier, A. Hourri, S. Natarajan, P. Benard, R. Chahine, Study of competitive adsorption of the N2O-CO2-CH4-N2 quaternary mixture on CuBTC, Sep. Purif. Technol. 235 (2020) 116211.

[19] S. Basu, A. C. Odena, I. F. J. Vankelecom, MOF-containing mixed-matrix membranes for CO2/CH4 and CO2/N2 binary gas mixture separations, Sep. Purif. Technol. 81 (2011) 31–40.

[20] N. A. Khan, S. H. Jhung, Facile syntheses of metal-organic framework Cu3(BTC)2 (H2O)3 under ultrasound, Bull. Korean. Chem. Soc. 30 (2009) 2921-2926.

[21] Y. K. Seo, G. Hundal, I.T. Jang, Y. K. Hwang, C. H. Jun, J. S. Chang, Microwave synthesis of hybrid inorganic–organic materials including porous Cu3(BTC)2 from Cu(II)-trimesate mixture, Microporous Mesoporous Mater. 119 (2009) 331–337.

[22] H. Yang, S. Orefuwa, A. Goudy, Study of mechanochemical synthesis in the formation of the metal–organic framework Cu3(BTC)2 for hydrogen storage, Microporous Mesoporous Mater. 143 (2011) 37–45.

[23] E. Biemmi, S. Christian, N. Stock, T. Bein, High-throughput screening of synthesis parameters in the formation of the metal-organic frameworks MOF-5 and HKUST-1, Microporous Mesoporous Mater. 117 (2009) 111–117.

[24] K. S. Lin, A. K. Adhikari, C.-N. Ku, C. L. Chiang, H. Kuo, Synthesis and characterization of porous HKUST-1 metal organic frameworks for hydrogen storage, Int. J. Hydrogen. Energy. 37 (2012) 13865–13871.

[25] A. Ahmed, M. Forster, R. Clowes, D. Bradshaw, P. Myers, &, H. Zhang, Silica SOS@ HKUST-1 composite microspheres as easily packed stationary phases for fast separation, J. Mater. Chem. A. 1 (2013) 3276-3286.

[26] M. Schlesinger, S. Schulze, M. Hietschold, M. Mehring, Evaluation of synthetic methods for microporous metal–organic frameworks exemplified by the competitive formation of [Cu2 (btc)3 (H2O)3] and [Cu2(btc)(OH)(H2O)], Microporous Mesoporous Mater. 132 (2010) 121-127.

[27] J. Klinowski, F. A. Almeida Paz, P. Silva, J. Rocha, Microwave-assisted synthesis of metal–organic frameworks, Dalton. Transactions. 40 (2011) 321-330.

[28] N. Missaoui, H. Kahri, U.B. Demirci, Rapid room-temperature synthesis and characterizations of high-surface-area nanoparticles of zeolitic imidazolate framework-8 (ZIF-8) for CO2 and CH4 adsorption, J. Mater. Sci. 57(2022) 16245-16257.

[29] N. Missaoui, A. Chrouda, H. Kahri, A. J. Gross, M. R. Ardani, P. A. Ling, M. Ahmadipour, PEG-templated synthesis of ultramicroporous n-ZIF-67 nanoparticles with

high selectivity for the adsorption and uptake of CO2 over CH4 and N2, Sep. Purif. Technol. 316 (2023) 123755.
[30] N. Missaoui, M. Bouzid, A. Chrouda, H. Kahri, H. Barhoumi, A. L. Pang, M. Ahmadipour, Interpreting of the carbon dioxide adsorption on high surface area zeolitic imidazolate Framework-8 (ZIF-8) nanoparticles using a statistical physics model, Microporous Mesoporous Mater. 360 (2023) 112711.
[31] I. Senkovska, F. Hoffmann, M. Fröba, J. Getzschmann, W. Böhlmann, S. Kaskel, New highly porous aluminium based metal-organic frameworks: Al(OH)(ndc) (ndc=2,6-naphthalene dicarboxylate) and Al(OH)(bpdc) (bpdc=4,4′-biphenyl dicarboxylate), Microporous Mesoporous Mater. 122 (2009) 93–98.
[32] H. R. Mahdipoor, R. Halladj, E. Ganji Babakhani, S. Amjad-Iranagh, J. Sadeghzadeh Ahari, Adsorption of CO2, N2 and CH4 on a Fe-based metal organic framework, MIL-101(Fe)-NH2, Colloids. Surf. A: Physicochem. Eng. Asp. 619 (2021) 126554.
[33] R. Banerjee, H. Furukawa, D. Britt, C. Knobler, M. O'Keeffe, O.M. Yaghi, Control of pore size and functionality in isoreticular zeolitic imidazolate frameworks and their carbon dioxide selective capture properties, J. Am. Chem. Soc. 131 (2009) 3875-3877.
[34] C. A. Fernandez, P. K. Thallapally, R. K. Motkuri, S. K. Nune, J. C. Sumrak, J. Tian, J. Liu, Gas-induced expansion and contraction of a fluorinated metal-organic framework Cryst. Growth. Des. 10 (2010) 1037–1039.
[35] B. Mu, F. Li, K. S. Walton, A novel metal–organic coordination polymer for selective adsorption of CO2 over CH4, Chem. Commun. 18 (2009) 2493-2495.
[36] Z. Liang, M. Marshall, A.L. Chaffee, CO2 Adsorption-Based Separation by Metal Organic Framework (Cu-BTC) versus Zeolite (13X), Energy Fuels. 23 (2009) 2785–2789.
[37] Z. Bao, L. Yu, Q. Ren, X. Lu, S. Deng, J, Adsorption of CO2 and CH4 on a magnesium-based metal organic framework, J. Colloid. Interface. Sci. 353 (2011) 549-556.
[38] Z. Bao, S. Alnemrat, L. Yu, I. Vasiliev, Q. Ren, X. Lu, S. Deng, Kinetic separation of carbon dioxide and methane on a copper metal–organic framework. J. Colloid. Interface. Sci. 357 (201) 504-509.
[39] A. R. Millward, O. M. Yaghi, Metal-Organic Frameworks with Exceptionally High Capacity for Storage of Carbon Dioxide at Room Temperature, J. Am. Chem. Soc. 127 (2005) 17998.
[40] R. Bose, J. P. Ethiraj, Sridhar, J. J. Varghese, N. S. Kaisare, P. Selvam, Adsorption of hydrogen and carbon dioxide in zeolitic imidazolate framework structure with SOD topology: Experimental and modelling studies, Adsorption. 26 (2020)1027-1038.

[41] S. K. Nune, P. K. Thallapally, A. Dohnalkova, C. Wang, J. Liu, G.J. Exarhos, Synthesis and properties of nano zeolitic imidazolate frameworks, Chem. Commun. 46 (2010) 4878–4880.

[42] J. Ethiraj, S. Palla, H. Reinsch, Insights into high pressure gas adsorption properties of ZIF-67: Experimental and theoretical studies, Microporous Mesoporous Mater. 294 (2020) 109867.

[43] M. Yan, Y. Zhang, N. Grisdanurak, H. Wibowo, C. Yu, E. Kanchanatip, CO2 adsorption on Cu-BTC to improve the quality of syngas produced from supercritical water gasification, Biomass. Conv. Bioref. (2022) 1-10.

[44] Y. Cao, Y. Zhao, F. Song, Q. Zhong, Alkali metal cation doping of metal-organic framework for enhancing carbon dioxide adsorption capacity, J. Energy. Chem. 23 (2014) 468-474.

[45] J. C. Súarez, V. C. Arias, H. I. Beltrán, A. T. Cruz, I. A. Ibarra, J. E. R. Ibarra, S. L. Serna, Synthesis and characterization of an SWCNT@HKUST-1 composite: enhancing the CO2 adsorption properties of HKUST-1, Acs Omega. 4 (2019) 5275-5282.

[46] H. R. Abid, G. H. Pham, H. M. Ang, M. O. Tade, S. Wang, Adsorption of CH4 and CO2 on Zr-metal organic frameworks, J. Colloid. Interface. Sci. 366 (2012) 120-124.

[47] T. Van Nguyen Thi, C.L. Luu, T.C. Hoang, T. Nguyen, T.H. Bui, P.H. Duy Nguyen, T.P. Pham Thi, Synthesis of MOF-199 and application to CO 2 adsorption, Adv. Nat. Sci. Nanosci. Nanotechnol. 4 (2013) 035016.

[48] J. Yang, R. Krishna, J. Li, J. Li, Experiments and simulations on separating a CO2/CH4 mixture using K-KFI at low and high pressures, Microporous Mesoporous Mater. 184 (2014) 21–27.

[49] K. Y. Andrew Lin, Y. T. Hsieh, Copper-based metal organic framework (MOF), HKUST-1, as an efficient adsorbent to remove p-nitrophenol from water, J. Taiwan. Inst. Chem. Eng. 50 (2015) 223–228.

[50] L. Li, X. L. Liu, H. Y. Geng, B. Hu, G. W. Song, Z. S. Xu, A MOF/graphite oxide hybrid (MOF: HKUST-1) material for the adsorption of methylene blue from aqueous solution, J. Mater. Chem. A. 1 (2013) 10292-10299.

[51] Z. Xiang, D. Cao, X. Shao, W. Wang, J. Zhang, W. Wu, Facile preparation of high-capacity hydrogen storage metal-organic frameworks: A combination of microwave-assisted solvothermal synthesis and supercritical activation, Chem. Eng. Sci. 65 (2010) 3140–3146.

[52] T. T. Li, J. Qian, Y. Q. Zheng, Facile synthesis of porous CuO polyhedron from Cu-based metal organic framework (MOF-199) for electrocatalytic water oxidation, RSC. Adv. 6 (2016) 77358-77365.

[53] K. S. W. Sing, D. H. Everett, R. A. W. Haul, L. Moscou, R. A. Pierotti, J. Rouquerol, T. Siemieniewska, Reporting Physisorption Data for Gas/Solid Systems with Special Reference to the Determination of Surface Area and Porosity, Pure Appl. Chem. 57 (1985) 603-619.

[54] M. Klimakow, P. Klobes, A. F. Thünemann, K. Rademann, F. Emmerling, Mechanochemical Synthesis of Metal-Organic Frameworks: A Fast and Facile Approach toward Quantitative Yields and High Specific Surface Areas, Chem. Mater. 22 (2010) 5216–5221.

[55] Y. Li, R. T. Yang, Hydrogen storage in metal-organic and covalent-organic frameworks by spillover, AIChE. J. 54 (2008) 269-279.

[56] P. Chowdhury, C. Bikkina, D. Meister, F. Dreisbach, S. Gumma, Comparison of adsorption isotherms on Cu-BTC metal organic frameworks synthesized from different routes, Microporous Mesoporous Mater. 117 (2009) 406–413.

[57] Q. Yu, Y. Tian, M. Li, Y. Jiang, H. Sun, G. Zhang, Z. Gao, W. Zhang, J. Hao, M. Hu, J. Cui, Poly (ethylene glycol)-mediated mineralization of metal–organic frameworks, Chem Comm, 56 (2020), 11078-11081.

[58] M. Wickenheisser, T. Paul, &, C. Janiak, Prospects of monolithic MIL-MOF@ poly (NIPAM) HIPE composites as water sorption materials. Microporous Mesoporous Mater, 220 (2016), 258-269

[59] M. G. Schwab, I. Senkovska, M. Rose, M. Koch, J. Pahnke, G. Jonschker, S. Kaskel MOF@ polyhipes. Adv. Eng. Mater, 10 (2008), 1151-1155.

[60] P. Ammendola, F. Raganati, R. Chirone, F. Miccio, Fixed bed adsorption as affected by thermodynamics and kinetics: yellow tuff for CO2 capture, Powder. Technol. 373 (2020) 446-458.

[61] K. Schlichte, T. Kratzke, S. Kaskel, Improved synthesis, thermal stability and catalytic properties of the metal-organic framework compound Cu3(BTC)2, Microporous Mesoporous Mater. 73 (2004) 81-88.

[62] J. R. Li, Y. Ma, M. C. McCarthy, J. Sculley, J. Yu, H. K. Jeong, H. C. Zhou, Carbon dioxide capture-related gas adsorption and separation in metal-organic frameworks, Coord. Chem. Rev. 255 (2011) 1791-1823.

718 [63] J. A. Mason, K. Sumida, Z. R. Herm, R. Krishna and J. R. Long, Evaluating metal–
719 organic frameworks for post-combustion carbon dioxide capture via temperature swing
720 adsorption, Energy. Environ. Sci. 4 (2011) 3030-3040.
721 [64] G. Ortiz, S. Brandès, Y. Rousselin, R. Guilard, Selective CO2 Adsorption by a
722 Triazacyclononane-Bridged Microporous Metal-Organic Framework, Chem. Eur. J. 17
723 (2011) 6689-669.
724 [65] Z. Zhang, Z. Li, J. Li, Computational study of adsorption and separation of CO2,
725 CH4, and N2 by an rht-type metal-organic framework, Langmuir. 28 (2012) 12122-12133.
726 [66] S. Keskin, High CO2 selectivity of a microporous metal–imidazolate framework: a
727 molecular simulation study, Ind. Eng. Chem. Res. 50 (2011) 8230-8236.
728 [67] J. Li, J. Yang, L. Li, J. Li, Separation of CO2/CH4 and CH4/N2 mixtures using MOF-
729 5 and Cu3(BTC)2, J. Energy. Chem. 23 (2014) 453–460.
730 [68] P. Chowdhury. C. Bikkina, S. Gumma, Gas adsorption properties of the chromium-
731 based metal organic framework MIL-101, J. Phys. Chem. C. 113 (2009) 6616−6621.
732 [69] D. Saha, Z. Wei, S. Deng, Hydrogen adsorption equilibrium and kinetics in metal–
733 organic framework (MOF-5) synthesized with DEF approach, Sep. Purif. Technol. 64
734 (2009) 280-287.
735 [70] Y. Liu, Is the free energy change of adsorption correctly calculated, J. Chem. Eng.
736 Data. 54 (2009) 1981–1985.
737 [71] B. Mu, P.M. Schoenecker, K.S. Walton, Gas adsorption study on mesoporous metal-
738 organic framework UMCM-1, J. Phys. Chem. C. 114 (2010) 6464–6471.
739 [72] J. R. Karra, K. S. Walton, Molecular simulations and experimental studies of CO2,
740 CO, and N2 adsorption in metal–organic frameworks, J. Phys. Chem. C. 114 (2010)
741 15735–15740.
742 [73] P. Aprea, D. Caputo, N. Gargiulo, F. Iucolano, F. Pepe, Modeling carbon dioxide
743 adsorption on microporous substrates: comparison between Cu–BTC metalorganic
744 framework and 13X zeolitic molecular sieve, J. Chem. Eng. Data. 55 (2010) 3655–3661.
745 [74] Q. M. Wang, D. Shen, M. Bülow, M. L. Lau, S. Deng, F.R. Fitch, N.O. Lemcoff, J.
746 Semanscin, Metallo-organic molecular sieve for gas separation and purification,
747 Microporous Mesoporous Mater. 55 (2002) 217–230.
748 [75] J. Möllmer, A. Möller, F. Dreisbach, R. Gläser, R. Staudt, High pressure adsorption
749 of hydrogen, nitrogen, carbon dioxide and methane on the metal-organic framework
750 HKUST-1, Microporous Mesoporous Mater. 138 (2011) 140-148.

751 [76] J. A. Dunne, M. Rao, S. Sircar, R. J. Gorte, A. L. Myers, Calorimetric heats of
752 adsorption and adsorption isotherms. 2. O2, N2, Ar, CO2, CH4, C2H6, and SF6 on NaX,
753 H-ZSM-5, and Na-ZSM-5 zeolites, Langmuir. 12 (1996) 5896-5904.
754 [77] S. Himeno, T. Komatsu, S. Fujita, High-pressure adsorption equilibria of methane
755 and carbon dioxide on several activated carbons, J. Chem. Eng. Data. 50 (2005) 369-376.
756 [78] J. R. Karra, K. S. Walton, Effect of open metal sites on adsorption of polar and
757 nonpolar molecules in metal-organic framework Cu-BTC, Langmuir. 24 (2008) 8620-
758 8626.
759 [79] E. G. Perez, J. Gascon, V. M. Florez, J. M. Castillo, F. Kapteijn, S. Calero,
760 Identification of adsorption sites in Cu-BTC by experimentation and molecular simulation,
761 Langmuir. 25 (2009) 1725-1731.
762 [80] S. Cavenati, C. A. Grande, A. E. Rodrigues, C. Kiener, U. Müller, Metal organic
763 framework adsorbent for biogas upgrading, Ind. Eng. Chem. Res. 47 (2008) 6333-6335.
764 [81] J. Duan, Y. Pan, G. Liu, W. Jin, Metal-organic framework adsorbents and membranes
765 for separation applications, Curr. Opin. Chem. Eng. 20 (2018) 122–131.